Numerical Studies on Crack Dilatancy of Concrete
II: Example of Practical Applications

Tsai-Fu Chuang

Department of Landscape Architecture, MingDao University

ABSTRACT

In this paper, a simple smeared crack dilatancy model is proposed. This model has been implemented into a FE program (LUSAS [1]) to investigate the influence of dilatancy effect. A single notched beam and a simple supported reinforced concrete beam subjected to transient impulsive loading were chosen for comparison. The numerical results have provided reasonable agreement with the experimental data. For the monotonic case, the influence of the dilatancy effect is more significant in the post-peak regime than in the pre-peak regime. For the impulsive loading case, the fundamental period increases when the dilatancy effect is considered.

Keywords: Dilatancy, Smeared crack model, Finite element method

混凝土裂縫膨脹性的數值模擬分析 II:應用與實例

莊財福

明道大學造園景觀系助理教授

摘要

本研究提出一個混凝土均散裂縫膨脹模式（smeared crack dilatancy model）。本模式已利用 Fortran 程式撰寫並與有限元素法程式（ＬＵＳＡＳ）連結。本文選擇單槽口樑（single notched beam）與鋼筋混凝土樑（Simple supported reinforced concrete beam）受到衝擊荷重之實驗資料做為驗證此模式之範例。分析結果顯示本模式數值結果與實驗結果相當吻合。而單槽口樑的分析結果並顯示，混凝土裂縫膨脹性的效果（dilatancy effect）在荷重－位移曲線(Load-Deflection Curve)的後頂區（post-peak regime）比前頂區（pre-peak regime）更為重要。而在鋼筋混凝土樑受到衝擊荷重分析結果顯示，震動週期會因為考慮了裂縫膨脹性的效果（dilatancy effect）而增加。

關鍵詞：膨脹，塗抹裂縫模式，有限元素法

I. INTRODUCTION

In this study, a single notched beam that is expected to have significant dilatancy effect was selected. This example was performed by CMSD-controlled (the CMSD is the Crack Mouth Sliding Displacement).The load-CMSD curves and the crack patterns obtained from experiment and numerical analysis are compared. The numerical crack patterns was also plotted to be further investigated. The second example relates to the mixed mode fracture test of a simple supported beam subject to transient impulsive loading. This work is intended to conduct a further investigation and gather more information of the dilatancy behaviour.

II. FINITE ELEMENT ANALYSIS

The LUSAS [1] finite element analysis package was used in this study. This program contains a material model interface (MMI) that allows users to develop computer code for material models then link the codes to the main program in such a way that the user code controls the material behaviour of the specified elements. With the help of this advanced package, the iterative scheme (i.e. Newton-Raphson or Modified Newton-Raphson method), the convergence criterion, and the arc-length method [2] needed to trace the softening curve can be easily adopted without expensive programming and testing. In this study, the iterative scheme adopted is the Newton-Raphson or Modified Newton-Raphson method, and the convergence criterion is the Euclidian residual norm [1]. Both of them are available in LUSAS and can directly be used without any programming. In LUSAS [1], the Euclidian residual norm r_ψ is defined by the norm of the residuals ψ as a percentage of the norm of the external forces R and is written as

$$r_\psi = \frac{\|\psi\|_2}{\|R\|_2} \times 100 \qquad (1)$$

where R contains the external loads and reactions. Owing to the inconsistency of the units of displacement and rotation, usually only translational degrees of freedom are considered

although all freedoms may optionally be included. In this study, a default value of $r_\psi = 0.1$ suggested by LUSAS user's manual is adopted.

2.1 Single notched beam

Among the experiments on mixed-mode concrete fracture, a single notched beam, tested by Arrea & Ingraffea [3], is selected for analysis. The supports and the loading conditions are non-symmetric with respect to the notch, as given in Fig. 1. The typical crack pattern is also given in Fig. 1. The test was performed by CMSD-controlled (the CMSD is the Crack Mouth Sliding Displacement). The material properties for the test are given in Tables 1.

The single notch beam is analysed with the fixed crack model first without and then with the dilatancy effect to investigate the influence of the dilatancy effect. Two-dimensional plane stress model with eight-noded plane stress elements (type QPM8) and six-noded plane stress element (type TPM6), see LUSAS User's Manual, were used to analyse the test specimens. The finite element mesh employed is this analysis is shown in Fig. 2 and 3.

Table 1 Concrete properties of single notch beam

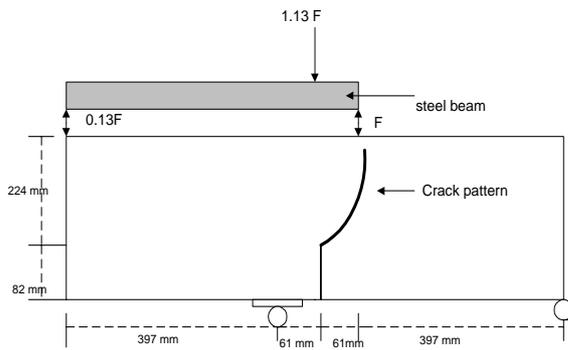|	
Young's modulus	E = 24800 N/mm^2
Poisson's ratio	ν = 0.2
Uniaxial compressive strength	f$_c$ = 28.0 N/mm^2
Uniaxial tensile strength	f$_t$ = 2.8 N/mm^2
Uniaxial strain at peak compressive strength	$\varepsilon_c^{'}$ = 0.0022
Fracture energy	G$_f$ = 0.07 N/mm
Initial shear retention factor	β = 0.1

Fig. 1. The typical crack pattern of experiment
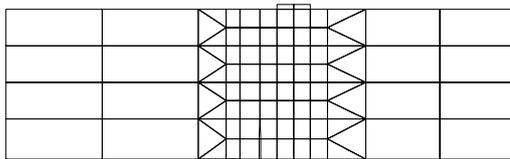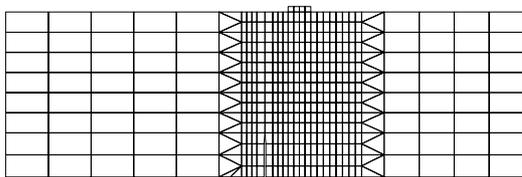

Fig. 2. Single notched beam. Mesh I

Fig. 3. Single notched beam. Mesh II

2.1.1 Mesh dependency study

The load-CMSD curves of the single notch beam obtained with the two meshes are shown in Fig. 4. It can be seen that the two finite element meshes give similar results. Based on this observation, all subsequent studies are performed using only mesh I. In the numerical analysis, the number of load increment is 30 and the number of iteration at each load step is shown in Table 2.

Table 2 Load increment and iteration of single notch beam

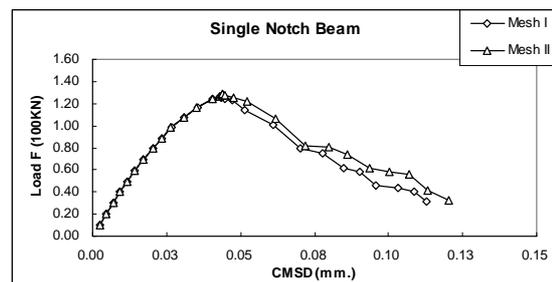| Load increment	Number of iteration	Load increment	Number of iteration
1	1	16	3
2	1	17	3
3	1	18	2
4	1	19	2
5	2	20	3
6	2	21	3
7	2	22	6
8	3	23	6
9	2	24	9
10	2	25	9
11	3	26	9
12	4	27	6
13	5	28	6
14	10	29	6
15	3	30	6

Fig. 4. Mesh dependency test ($\mu = 0.0$)

2.1.2 Load-CMSD curves

Two different values of the dilatancy parameter ($\mu_1 = 0.3$ and 0.5) are used to show the influence of dilatancy effect on the load-CMSD curves. The load-CMSD curves obtained with non-dilating ($\mu_1 = 0.0$), simple dilatancy model and experimental results are shown in Fig. 5.

Fig. 5 shows that the load-CMSD curves obtained from the experiment and the numerical model ($\mu_1 = 0.0$, 0.3 and 0.5) are in reasonable agreement. In addition, it can be seen that the influence of the dilatancy effect is more significant in the post-peak regime rather than that of the pre-peak regime as expected. Additionally, in the post-peak regime, it can be observed that the dilatancy effect has the obvious influence.
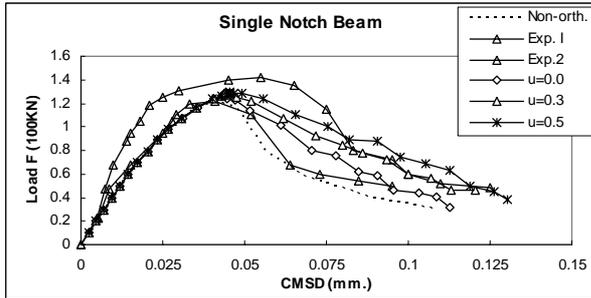
Fig. 5. Load F versus CMSD of single notch beam
("u" represents dilatancy parameter (μ_1))

2.1.3 Non-orthogonal crack model

In order to compare the results obtained from the simple dilatancy model (fixed crack) with other crack models, the non-orthogonal crack model [4] available in LUSAS is also used with the same material parameters used by the simple dilatancy model. Fig. 5 also provides a load-CMSD curves obtained from the non-orthogonal model. By comparing the results obtained from the non-orthogonal model and the experiment, it can be seen that the non-orthogonal model shows a reasonable agreement with one of the experimental results. However, by comparing the results obtained from the fixed crack model ($\mu_1 = 0.0$) and the non-orthogonal model (non-dilatat), it can be seen that the results differ greatly. The main reason could be that the criteria to account for shear transfer to cracked surfaces employed in these two models are different and therefore, lead to a different result.

2.1.4 Crack pattern

Since the influence of the dilatancy effect on the numerical crack pattern is very minor, only the crack pattern obtained from the non-dilating model is given, as shown in Fig. 6.

In the pre-peak regime, i.e. from 1st load increment to 20th load increment, the cracks initially appeared on the above right of the notch. With the increase of loading, the cracks propagate in a curvilinear way and then continues to propagate in a vertical direction. The numerical crack pattern obtained in this study shows good agreement with other smeared crack model [5]. However, the experimental crack pattern (Fig. 1) shows a larger change in propagating direction than the numerical crack pattern.

The comparison between the numerical and experimental crack patterns shows that the maximum principal stress criterion adopted in the current crack model can predict the crack initiation well but needs to be improved in the prediction of the crack propagation.
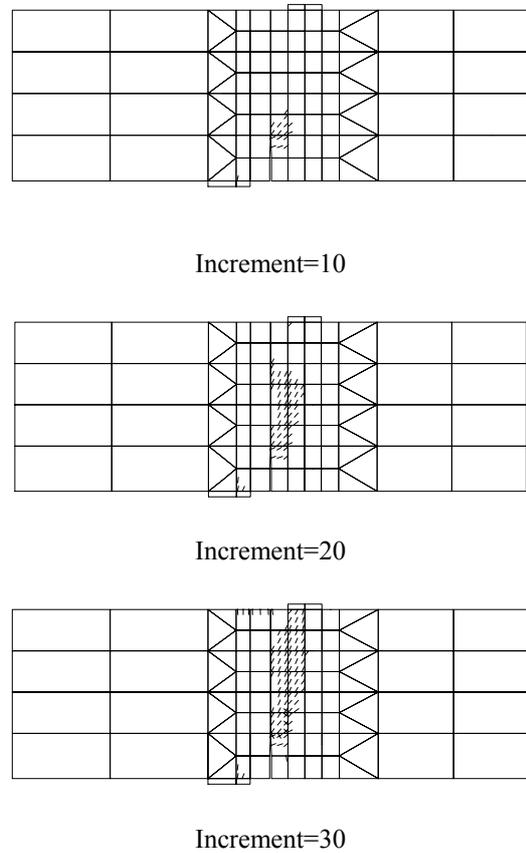

Increment=10

Increment=20

Increment=30

Fig. 6. Numerical crack patterns

2.2 Simply Supported beam

A simply supported reinforced concrete beam investigated by Beshara and Virdi [6] is selected for analysis. This reinforced concrete beam shown in Fig 7 is subjected to two symmetrically applied concentrated loads which are applied as step loads with a zero rise time (Fig. 8). The beam is reinforced in the lower

position by 1290 mm². The material properties are listed in Tables 3 and 4

Two-dimensional plane stress models are used to analyse the test specimens. Due to the symmetry, only one half of the specimen was modeled using eight-noded isoparametric elements (QPM8) with axial bars (BAR3) to simulate the reinforcing steel. The dynamic analysis is performed with a time step of 0.002 sec.

Table 3 Concrete properties

Initial Young's modulus	$E_0 = 42059$ N/mm²
Poisson's ratio	$\nu = 0.2$
Mass density	1932 kg /m³
Uniaxial compressive strength	$f_c = 25.8$ N/mm²
Uniaxial tensile strength	$f_t = 3.2$ N/mm²
Uniaxial strain at peak compressive strength	$\varepsilon_c' = 0.0023$
Fracture energy	$G_f = 0.1$ N/mm
Initial shear retention factor	$\beta = 0.1$

Table 4 Steel properties

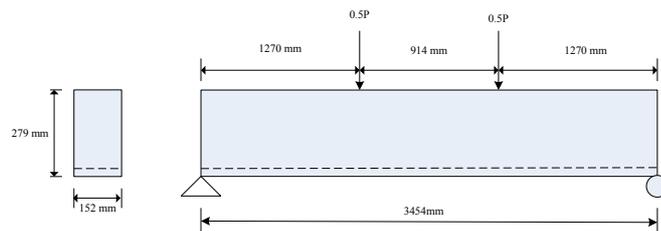| Initial Young's modulus	$E_0 = 206850$ N/mm²
Poisson's ratio	$\nu = 0.2$
Mass density	6535 kg/m³
Yield stress	$\sigma_f = 303$ N/ mm²
Hardening parameter	$H = 15000$ N/mm²

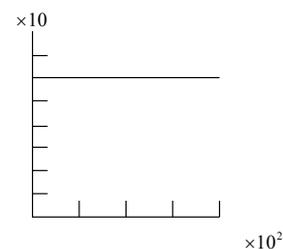Fig. 7. Beam geometry and dimensions (mm.)

Fig. 8. Loading time history

2.2.1 Step-by-step dynamic analysis

In this study, both the linear and non-linear step-by-step dynamic analyses have been selected. The incremental equations of dynamic equilibrium can be presented as

$$M \ddot{\Delta d} + C \dot{\Delta d} + K_T \Delta d = \Delta Q \qquad (2)$$

where Δd, $\dot{\Delta d}$ and $\ddot{\Delta d}$, and are the increments of displacement, velocity and acceleration vectors during the time step Δt, respectively. M, C and K_T are the mass, damping, and tangent stiffness matrix, respectively. ΔQ are the increments of external loads during the time step Δt.

No viscous damping has been considered by Beshara and Virdi [6] and this study; therefore, equation (2) can be simplified to be:

$$M \ddot{\Delta d} + K_T \Delta d = \Delta Q \qquad (3)$$

2.2.2 Mesh dependency study

Two finite element meshes are used to show the influence of mesh refinement on the nonlinear response curves of the simple supported beam

which are shown in Figs. 9 and 10. The nonlinear response curves obtained with the two meshes are shown in Fig. 11. It can be seen that the two finite element meshes give similar results. In the numerical analysis, the number of time step is 25 and the number of iteration at each time step is shown in Table 5. In this study, the iterative scheme adopted is the Newton-Raphson or Modified Newton-Raphson method, and the convergence criterion is the Euclidian residual norm [1]. Both of them are available in LUSAS and can directly be used without any programming.

Table 5 Time step and iteration of simple
supported beam

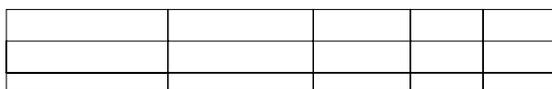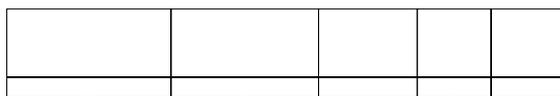| Time step	Number of iteration	Time step	Number of iteration
1	1	14	2
2	1	15	2
3	1	16	2
4	1	17	1
5	1	18	1
6	4	19	1
7	4	20	1
8	3	21	1
9	2	22	1
10	3	23	2
11	2	24	1
12	2	25	1
13	2		

Fig. 9. Simple supported beam. Mesh I

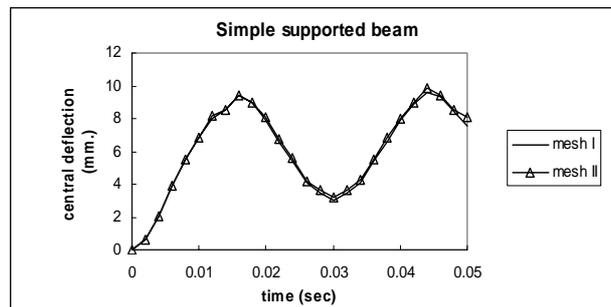Fig. 10. Simple supported beam. Mesh II
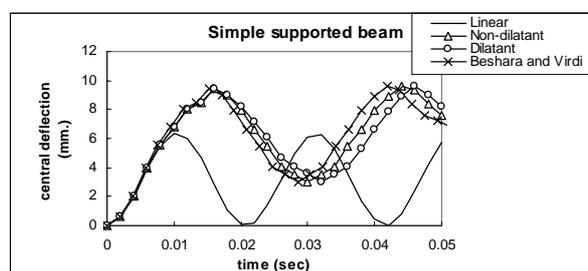

Fig. 11. Mesh dependency study

Fig. 12. The linear and nonlinear response
(Non-dilatant and Dilatant) of the beam

2.2.3 Span-deflection response

An elastic analysis was first carried out as a check, and the results were found to be in excellent agreement with those given by Beshara and Virdi [5]. Fig. 12 shows the time history of the mid-span deflection for the linear case and the nonlinear analysis cases representing the proposed model and that given by Beshara and Virdi [5]. The central deflection history of the nonlinear case of this study was found to be reasonable agreement with that given by Beshara and Virdi [5].

Fig. 12 also shows that the amplitude is not affected by the dilatancy effect. However, the fundamental period increases when the dilatancy effect is considered.

In order to trace the possible reason to explain this behaviour, the dynamic equilibrium equations (Eq.4) used for the step-by-step analysis is reviewed. In a step-by-step dynamic analysis, the stiffness matrix [K], mass matrix [M] and damping matrix [C] are the three properties of a structure which potentially affect the whole dynamic behaviour. In this study, a constant mass density is used and this will lead to a constant mass matrix [M]. Additionally, as reported in the

previous section, the viscous damping is not considered in this study. Therefore, it is obvious that a possible reason can be that the magnitude of the stiffness matrix [K] is affected when the dilatancy effect is taken into account. Since the geometrical nonlinearity is not considered in this study, the strain-displacement matrix [B] is kept as a constant matrix. It is known that the stiffness matrix [K] can be represented as $[K] = \int [B]^T [D][B] d\Omega$; therefore, the only component which will affect the value of the stiffness matrix is the tangential D-matrix. One possible explanation is that when the dilatancy effect is taken into account, it will lead to a different tangential D-matrix, and therefore, lead to a different stiffness matrix [K]. This should be further investigated in future work.

From Fig. 12, the following conclusions can be drawn regarding the linear and nonlinear responses:

1. An increase of the maximum deflection in the nonlinear case by almost 50% than in the linear elastic case (i.e. 9.3mm/6.2mm=1.5).
2. An elongation of the fundamental period in the nonlinear case by almost 50% than in the linear elastic case (i.e. 0.03sec/0.02sec=1.5).

2.2.4 Numerical Crack pattern

The crack patterns obtained from the numerical analysis of mesh II are given in Fig 13.

It can be seen that the cracks initially appeared at the middle-bottom area of the beam. This is because the flexural deformations produce the cracks which are all perpendicular to tension face at initiation. As the cracks propagate further into the beam, the compressive strain, combined with the shear strain, alters the inclination of the principal strain so that they incline towards the horizontal. The predicted patterns in the present analysis were found to be in good agreement with that given by Beshara and Virdi [5].

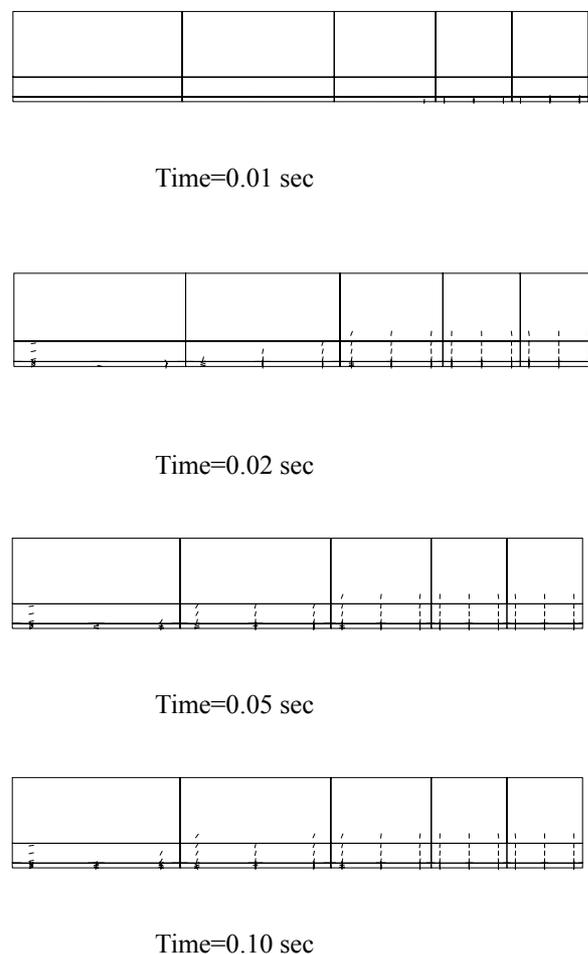Time=0.01 sec

Time=0.02 sec

Time=0.05 sec

Time=0.10 sec

Fig. 13. Simple supported beam. Crack pattern of Mesh II

III. CONCLUSION

In this paper, the performance of the dilatancy effect in concrete cracking is assessed by analysing a single notch beam and a reinforced concrete beam. Several conclusions can be drawn regarding the numerical analysis and the experimental result.

1. For the monotonic case, the influence of the dilatancy effect is more significant in the post-peak regime than in the pre-peak regime. This is because not many cracks occur at the pre-peak zone and therefore dilatancy is not active.
2. The crack patterns obtained from the non-dilatant model and simple dilatancy model do not differ much. The reason is that the maximum principal stress criterion

governs the crack initiation and propagation. Although the dilatancy law will begin to be active after crack initiation, the results show that it does not affect the crack propagation.

3. For the impulsive loading case, an increase of the maximum deflection in the nonlinear case by almost 50% than in the linear elastic case. Also, an elongation of the fundamental period in the nonlinear case by almost 50% than in the linear elastic case. In addition, the fundamental period increases when the dilatancy effect is considered.

REFERENCES

[1]   FEA Ltd. Lusas User Manual , London, England, 2007.

[2]   de Borst, R. "Computation of post-bifurcation and post-filure behavior of strain-softening solids." Computers and Structures, Vol. 25, No. 2, pp.211-224. , 1987.

[3]   Arrea, M., and Ingraffea, A. R. . "Mixed-mode crack propagation in mortar and concrete." Report 81-13, Department of Structure. Engineering. Cornell University, Ithaca, New York, 1982.

[4]   de Borst, R., and Nauta, P. . "Non-orthogonal cracks in a smeared finite element model." Engineering and Computations, Vol. 2, pp. 35-46, 1985.

[5]   Rots, J. G., Nauta, P., Kusters, G. M. A., and Blaauwendraad, J. "Smeared crack approach and fracture localization in concrete." Heron, Vol. 30, No. 1, pp.1-48, 1985.

[6]   Beshara, F. B. A., and Virdi, K. S.. "Non-Linear Finite Element Dynamic Analysis of Two-Dimension Concrete Structures." Computers and Structures, Vol. 41, pp. 1281-1294, 1992.